UNIVERSITY of CALIFORNIA
SANTA CRUZ

INVESTIGATION OF SILICON SENSOR STRIP NOISE ON LONG LADDERS

A thesis submitted in partial satisfaction of the
requirements for the degree of

BACHELOR OF SCIENCE

in

PHYSICS

by

Sean C. H. Crosby

10 June 2009

The thesis of Sean C. H. Crosby is approved by:

Professor Bruce Schumm
Technical Advisor

Professor David P. Belanger
Thesis Advisor

Professor David P. Belanger
Chair, Department of Physics

Abstract

Investigation of Silicon Sensor Strip Noise on Long Ladders

by

Sean C. H. Crosby

The equivalent charge noise for long ladder silicon strip sensors is examined in this paper. It is found to deviate from standard estimation formulae. To simulate a long ladder detector many strips on a single detector were connected in a serpentine arrangement. The equivalent charge noise measured for this long ladder detector was much lower than expected, despite the rigorous estimation techniques used involving shaper and amplifier constants. These results suggest that there are effects not yet understood for long ladder silicon sensors.

Contents

List of Figures

To my Parents, for always supporting me not matter what my interest is.

To my Brother, who will always listen.

Acknowledgements

I would like to thank;

My thesis advisor, Bruce Schumm. Without your support I would have never finished this paper or got to work on such an interesting project.

Vitality Fadeyev. Without your help, support and vast knowledge and know-how none of this would be possible.

Forest Martinez-McKinney. For many countless and beautiful wirebonds, and lots of technical advice.

Max Wilder. For guidance and very practical help.

LTSFE2 team. For making it a fun and interesting time.

1 Motivation

The International Linear Collider (ILC) will be the worlds highest energy electron-positron collider. It will accelerate electrons and positrons to produce center-of-mass energies of 500GeV. The ILC will be used to precisely study new forces and matter states discovered at the Large Hadron Collider (LHC). It is currently in the design phase, and the community has not yet decided on a detector concept. Of the three proposed concepts, in particular, the SID concept utilizes solid-state silicon tracking, and a silicon-tungsten sampling calorimeter. The detector will be composed of many different kinds of detector layers. The vertex layers are approximately 1.5-7cm from the collision while the tracking layers will be about 20-125cm from the collision (see Fig. 1.1). These layers could have sensor lengths that correspond roughly with their radial distance from the collision. Current efforts to design an efficient and highly accurate tracking system include long ladders, charge division, and double metal technologies.

Long ladder detector systems will provide a tracking solution that use sensors daisy chained into ladders approximately 80cm in length. Utilizing long ladders will reduce cabling, readout boards, and heat from electronics. Less material between sensor arrays will mean less uncertainty due to trajectory distortion from scattering inside material, and therefore more accurate momentum measurements. The ILC beam is planned to cycle at five Hertz (1ms on, 199ms off). The magnetic field inside the detector will be five Tesla, meaning therefore, that every conductor with a current will feel a significant force. Due to the beam cycling, the detector systems power will cycle as well, leading to a non-constant force on all the electronics. By limiting the amount of readout electronics

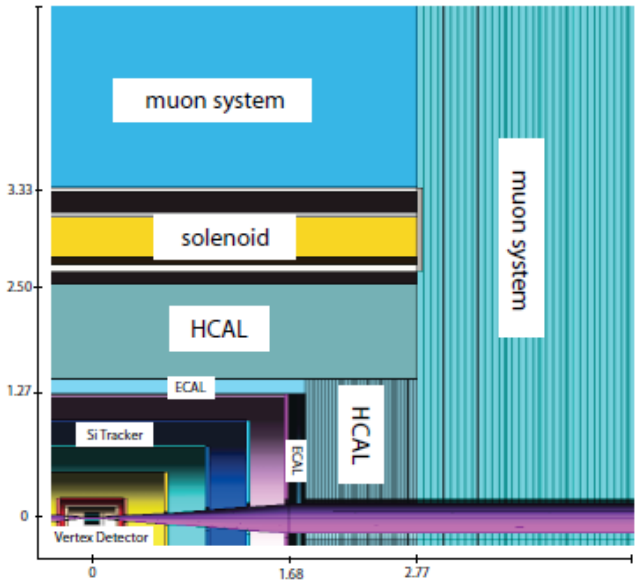

Figure 1.1: An illustration of a single quadrant of the SID detector design. Length scale shown above is in meters.[2]

this periodic "hammering" force will be reduced. The reduction of material will also produce more accurate calorimeter measurements due a reduced amount of photon conversion.

While a long ladder detector system provides many solutions, the accuracy of signal measurements is not well known. As readout strip length increases, so does the strip capacitance and resistance. Because the tracking system needs to be extremely accurate, very narrow strips with very fine pitches are used. The strips themselves are approximately 7um wide, and their pitch (the distance between two strips) is 50um. These narrow strips have a large resistance (3KOhms for 80cm) leading to a potentially large readout noise. This noise contribution from strip resistance does not increase linearly with length. In fact, the noise contribution is expected to increase as length$^{(3/2)}$. This can be seen from the noise estimation equation, Eq. 1.1, derived Helmuth Spieler [1]. Q is noise in electrons. I_d, R_b, R_s, and C are sensor characteristics referring respectively to leakage (quiescent) current, bias resistance, strip resistance, and strip capacitance. The shaping factors F_i and F_v, and are of order one and the time constant τ is a measure of pulse shaping. These are discussed in section 3.3.

$$Q^2 = F_i\tau(2eI_d + \frac{4kT}{R_b} + i_{na}^2) + \frac{F_v C^2}{\tau}(4kTR_s + e_{na}^2) + 4F_v A_f C^2 \text{ [SI Units]} \tag{1.1}$$

As seen in Eq. 1.1 the strip resistance term, R_s is multiplied by C^2. Because resistance and capacitance are both proportional to length, $Q^2 \sim l^3$ or $Q \sim l^{3/2}$. This non-linearity is my focus of concern. As the signal-to-noise ratio is critical to understanding the achievable positional resolution for high energy particles, the question of whether this approximate equation is valid at long length scales is very important. This is where an experimental study is needed.

2 Background

2.1 Silicon Sensors

Silicon sensors are used to detect ionizing particles. They are used in a variety of settings including radiation and photon detection. Because they are solid state devices that work at high speed they can be very accurate, they are ideal candidates for detection systems in particle accelerators.

The common AC-coupled sensor will be the focus of my study. It can be described in simplest terms a diode. Commonly n-type silicon is used for the bulk of the sensor, and p-type silicon is implanted in long strips on the bulk surface (see Fig. 2.1). The bulk will get a metalization layer on its backside, and the p-type strips will get an insulating layer of silicon oxide on their topside. Aluminum strips will be placed on top of the silicon oxide creating a capacitor with the p-type implant. As a protective measure, a passivation layer is deposited on top of the entire sensor leaving exposed pads for wire bonding connections.

By applying a positive potential to the backside metalization and connecting the p-type implants to ground via a bias resistor, a reverse bias is applied to this diode. The depletion region will increase as a greater potential is applied. If a large enough potential is applied the entire n-type bulk will be completely depleted, and therefore free of any charge carriers. As shown in Fig. 2.1, an electric field is generated inside the bulk by the potential difference. Because most sensors deplete at or before 100V, this is the bias voltage used for my studies. This configuration is ideal for detecting

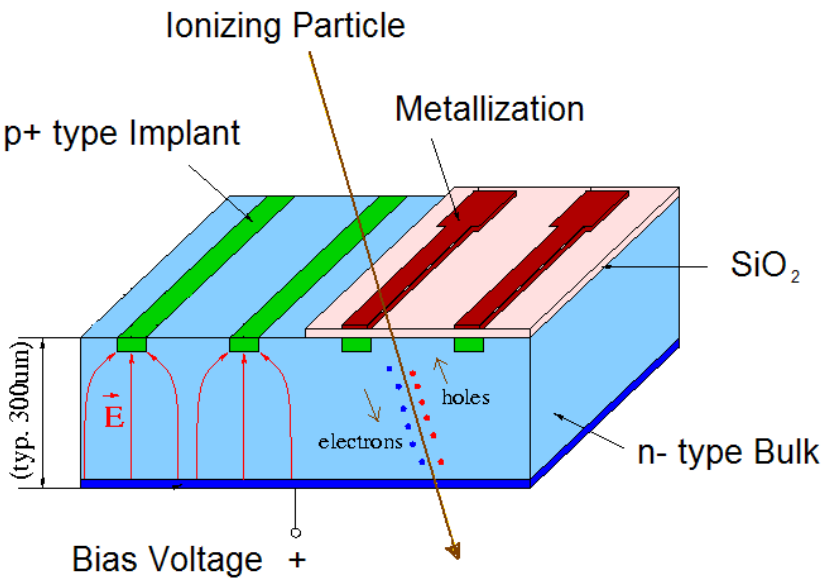

Figure 2.1: Illustration of basic functioning of an AC-biased silicon sensor.

ionizing particles which free approximately 24,000 electrons as they pass through the sensor.

As ionizing particles from ILC collisions pass through the bulk of the sensor they leave a trail of electron-hole pairs behind. Before these charges recombine they are separated by the electric field created by the applied potential difference (100V). In the electic field, the electrons move towards the positive voltage and the holes move towards the negative voltage, therefore creating an excess charge on both the p-type implant and metalized bottom of the sensor. The excess charge on the top can be read out via the capacitive link between the aluminum strip and p-type implant. By examining which strips detect hits, the position of the ionizing particle can be measured. A detector system for a collider will generally have lots of layers of silicon sensors to determine the particle's trajectory.

Using the particle's trajectory, a very important quantity, the particle's momentum, p, can be derived. Inside the detector a very strong 5 Telsa magnetic field is present. Because a moving

charged particle in a magnetic field will feel a force perpendicular to its velocity, the ionizing particles from collisions will follow a curved trajectory as they leave the detector. The momentum can be determined by measuring the radius of this curvature of the trajectory as seen below.

$$r[m] = \frac{p * c}{300B} \left[\frac{MeV}{Tesla}\right] \tag{2.1}$$

Here, r is radius, p is momentum, c is the speed of light, and B is the magnetic field.[3]

The ILC will be designed to examine very high energy particles that, despite the strong magnetic field, will have very large radii of curvature. The ability to measure this slight curvature is crucial in making accurate momentum measurements. Using a strip pitch of 50um, position can be determined to better than 10um by examining the distribution of charge left by the ionizing particle. This ability to measure this charge signal accurately is essential to achieve a high position resolution that results in an accurate momentum measurements.

2.2 Noise

Electronic noise is random fluctuations in the amplified signal due to a variety of effects. These fluctuations obscure the signal and can degrade the quality of the data provided by the sensor. The most important influence of noise is the signal-to-noise ratio. This ratio provides a figure of merit used to determine the amount of information one can derive from a signal.

Electronic noise can be thought of as fluctuations in current. This leads to two statistically independent sources: he velocity fluctuations of electrons, and the number fluctuations of electrons. Velocity fluctuations come from thermal motion of atoms in the conducting material. This jostling yields a large dispersion of velocities. The number fluctuation in electrons is due to many different sources such as thermionic emission or carrier generation and recombination.

The primary focus of this experiment will be thermal noise, but to understand our noise measurements, all noise sources of our silicon sensor must be understood and approximated. Thermal noise, commonly referred to as "Johnson noise", arises due to velocity fluctuations in resistors. In the

voltage regime, or for series resistance, the noise density is proportional to resistance (See Eq. 2.2). In the current regime, or for parallel resistance, the spectral noise density is inversely proportional to resistance (See Eq. 2.3). Spectral noise density is the noise measured per unit of bandwidth. These equations are derived for example by Helmuth Spieler[1].

$$e^2 = 4kTR \tag{2.2}$$

$$i^2 = \frac{4kT}{R} \tag{2.3}$$

Shot noise is another important noise source arising due to number fluctuations. Shot noise arises due to charge carriers injected independently of one another. Because the silicon sensor is essentially a diode it is subject to dark current. Dark current is a small reverse current through a diode due to quantum fluctuations arising from the Boltzmann distribution of carrier energies. This Dark current is genearlly characterized as 'leakage' current. These fluctuations are increased by the large reverse bias voltage applied to the sensor and these release times generally follow a Poisson distribution. This leads to a spectral noise density proportional to the current(I) generated by additional carriers (see Eq. 2.4).

$$i^2 = 2eI \tag{2.4}$$

A third noise source, commonly called 1/f noise, occurs when fluctuations are not random. Carrier trapping and release is a good example of this noise type. Carriers are trapped with various release lifetimes. An effectively infinite, uniformly distributed set of trapping times yield a power density inversely proportional to frequency (f). Because the noise contribution is larger when f is small, this is sometimes called low frequency noise.

To estimate the noise from the sensor, all these noise sources must be combined and integrated over the entire frequency spectrum. Derivations in [1] show the noise measured for a sensor of characteristics I_d, R_b, R_s, and C and amplifier characteristics i_{na}, e_{na}, A_f. This derivaiton is shown by Eq. 1.1 and here as Eq. 2.5 for convenience. The shaping factors F_i and F_v, and the time constant, τ, come from the shaping characteristics of the amplifier used to read out the sensor. They

are discussed in section 3.3.

$$Q^2 = F_i\tau(2eI_d + \frac{4kT}{R_b} + i_{na}^2) + \frac{F_v C^2}{\tau}(4kTR_s + e_{na}^2) + 4F_v A_f C^2 \text{ [SI Units]} \tag{2.5}$$

This equation yields a noise estimate in Coulombs(C). It is helpful to compare the noise with the signal expected for an ionizing particle. The more comparable the noise is to the signal, the less information can be gathered. Generally, signal-to-noise ratios are referenced, and a very high signal-to-noise ratio is desired. For detector systems in particle accelerators the desired signal-to-noise ratio is generally at least 10.

I_d is the leakage current through the sensor while it is biased. Generally this leakage increases as the bias voltage increases, flattening off at a characteristic voltage. Somewhere above this voltage the P/N junction in the sensor breaks down and the current increases exponentially. On a working sensor this break down occurs far from the full depletion voltage. For our sensor the current leakage was about 0.30uA at a 100V bias. This is the leakage current measured for the entire sensor and therefore the leakage current through each strip is .30uA/128 strips, or approximately 2.3nA/strip.

R_b is the value of the bias resistor connecting the implant(s) to ground potential. A fairly high resistance of value 40 MΩ was used to keep the noise contribution from the bias resistor low. R_s is the total resistance of the readout strip. To increase the effect of strip resistance we chose a sensor with narrow strips (7.5um width) each with resistance 276Ω.

C represents the strip capacitance dominated by the its nearest neighbors, but also includes contributions from the backplane as well. By grounding neighboring strips in our experiment, this inter-strip capacitance was well defined. In a typical sensor setup all strips are connected to the amplifier. This connection is nearly ground due to the low impedance (1-2KΩ) of the amplifier[1]. For noise measurements in the test setup, defining the neighboring strips is neccessary to replicate a working sensor. The capacitance was measured to be approximately 1.1pF/cm for the sensor used.

For this study, the term of greatest interest in Eq. 2.5 is: $\frac{F_v C^2}{\tau} 4kTR_s$. The magnitude of

[1]Ned Spencer, Engineer, SCIPP. Private communication

this term is determined by the strip resistance and capacitance. Its effect on long ladders may be severe due to its nonlinear dependence on strip length. Strip resistance and capacitance are both proportional to strip length(l) yielding a relationship to noise: $Q^2 \sim l^3$ or $Q \sim l^{3/2}$. Therefore as strip length increases this term becomes the dominating noise source, and is my primary concern in this study.

In prior experiments with short or wide strip sensors, the noise generated by strip resistance(strip noise) was not a large consideration due to its small effect. Exact shaper constants, F_i and F_v, had small effects on the total noise. Initially I naively used this simplified equation based on a CR-RC shaper with shaper constants, $F_v = F_i = .924$, linearily combined with Eq. 2.7. Equation 2.7 represents strip noise, and was estimated with the same CR-RC shaper constants.

$$Q^2 = 12\left[\frac{e^2}{nA * ns}\right] I_d\tau + 6 * 10^5\left[\frac{e^2 k\Omega}{ns}\right]\frac{\tau}{R_b} + 3.6 * 10^4\left[\frac{e^2 ns}{(pF)^2(nV)^2/Hz}\right] e_n^2\frac{C^2}{\tau} \tag{2.6}$$

$$Q^2 = \frac{F_v 4kTR_sC^2}{\tau}[\text{SI Units}] \tag{2.7}$$

For single strip length measurements this combined equation (added in quadrature) agreed very well. Only when longer strip lengths were examined, did the importance of Eq. 2.5 become apparent. Prior to examining Eq. 2.5 I was unaware that the shaping factors had such a large effect at long strip lengths. Therefore, to achieve better estimates for long ladder sensor chains, amplifier characteristics will need to be well known. These characteristics are discussed in section 3.3.

3 Materials and Method

3.1 Readout Electronics

Reading out the excess charge generated on the strips of the sensor by an ionizing particle requires well designed amplification and shaping electronics. Because the charge is very small, electronic noise arising in the amplification of the signal is a highly significant issue. An diagram of the measurement systems functionality is show in Fig. 3.1.

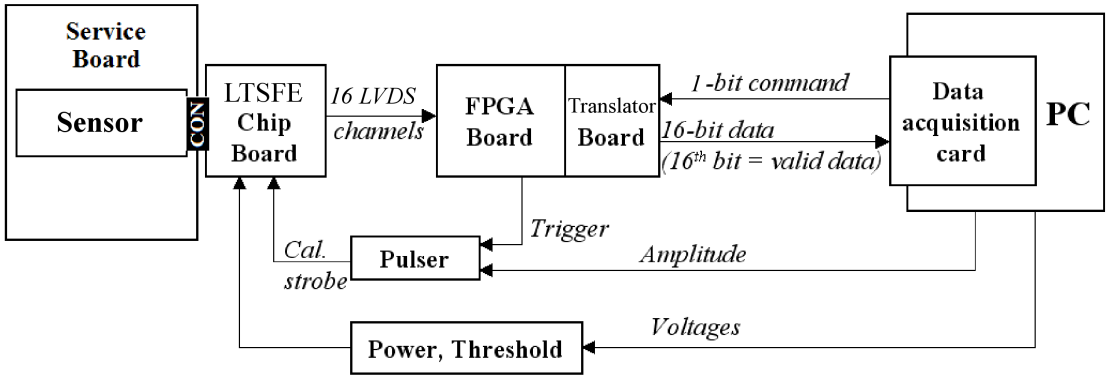

Figure 3.1: An overview of the setup components and basic functionality hierarchy.

The process begins with the amplifiers on the LTSFE Chip Board (front-end). The signal charge is run through three amplification stages that are designed to amplify the signaland filter the noise. The last two stages shapes the signal using differentiation and integration circuitry (shaping is discussed in section 3.3). The amplified signal is then presented to the comparator, which which

provides an output signal ("hit") when its input exceeds a pre-defined threshold. These hits are then sent in the low voltage differential signal (LVDS) standard to the FPGA board. Hits are read out through the connecting board to a data acquisition card on the PC (see Fig. 3.1).

Power and threshold voltages are supplied to the front end board by a stack of power supplies. Because it is not easy to direct ionizing particles at the sensor strips with high spatial precision, a pulser is used to produce the charge on readout lines. A 1pF capacitor is connected serially in line to the reaout strip to transform the voltage signla provided by the pulser into a charge. These power supplies and pulser are controlled by the PC using the General Purpose Interface Bus (GPIB). The pulser is also triggered by the FPGA (see Fig. 3.1).

3.2 Noise Measurements

The occupancy method was used to make noise measurements in this study. The idea behind this method is the generation of S-curves. An S-curve is plot of occupancy versus threshold. Given a particular threshold voltage established by a power supply, a set number of pulses are generated and then readout through the comparator. The FPGA then sends the number of hits recorded at that threshold to the comparator. This number of hits divided by the total pulses sent is the occupancy. Given a noiseless system, if the threshold voltage is less than the voltage of the input pulse, we would expect to record the same number of hits and pulses sent. Even in a normal noisy setting, if the threshold is low enough, occupancy is 100%. By varying the threshold below and above the voltage of the input pulse, an S-curve is generated (see Fig. 3.2).

The derivative of the S-curve follows a Gaussian distribution. The 50% occupancy level corresponds to the peak of the Gaussian and the Gaussians width corresponds to the characteristic width of the S-curve. A very steep S-Curve means a very sharp Gaussian peak and therefore a low noise, while a shallow S-curve means a very wide Gaussian peak corresponding to high noise. The threshold position of 50% occupancy represents the input signal measured after amplification. This happnes, because on average, half the time noise will bring the signal below threshold and half the

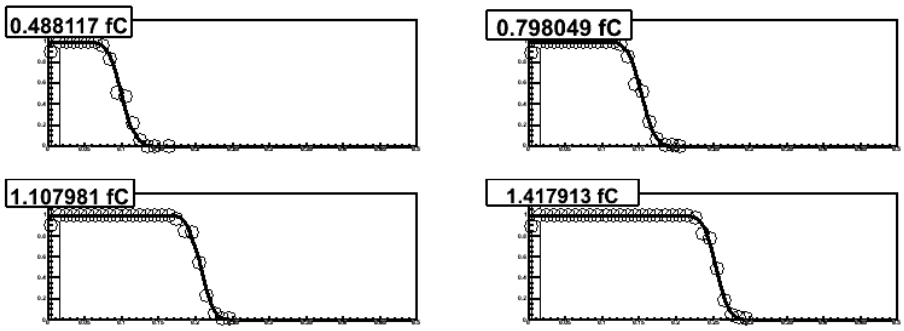

Figure 3.2: Different S-curves for different input charges. X-axis is threshold. Y-axis is occupancy.

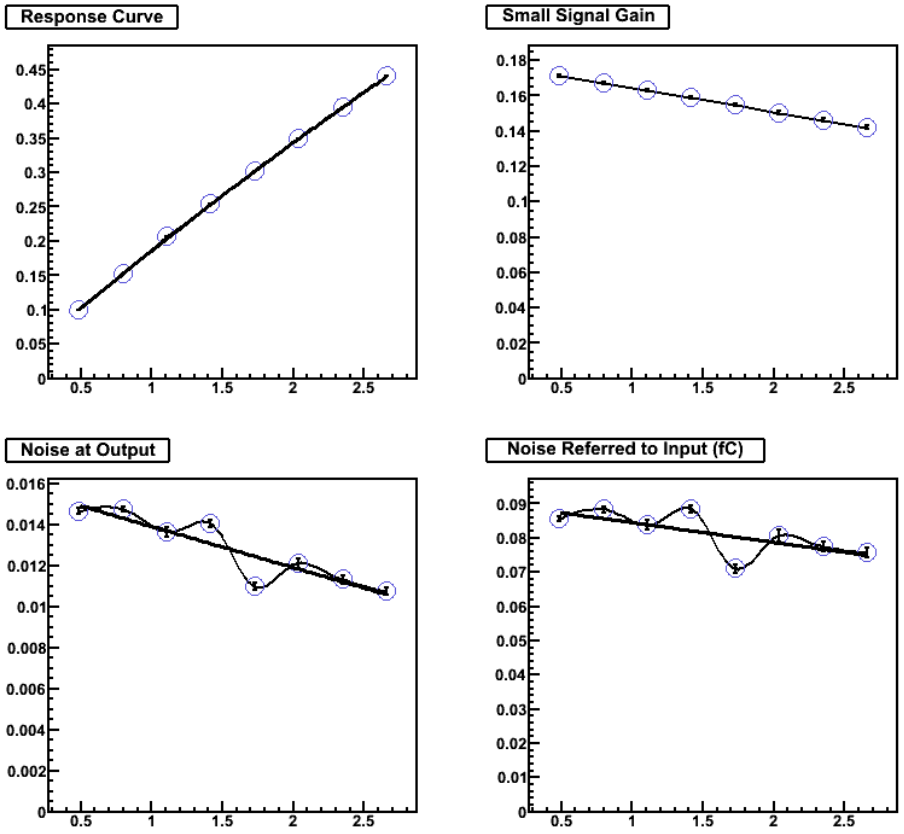

Figure 3.3: Top left: x-axis is input charge, y-xis is response voltage. Top right: x-axis is input charge, y-axis is small signal gain (dV/dQ). Bottom left: x-axis is input charge, y-axis is RMS-noise. Bottom right: x-axis is input charge, y-axis is (RMS noise)$*dQ/dV$.

time noise will bring the signal above the threshold. To measure the gain of the system I took this voltage and referenced it against the input charge as seen the response curve in Fig. 3.3. Taking the

derivative of the response curve (dV/dQ) yields the small signal gain also shown in Fig. 3.3.

The noise at amplifier's output is measured as the width of the S-curve transition. The value plotted against the input charge is shown as Noise at Output in Fig. 3.3. To translate this value to the noise that would have been on amplifier's input, I divide it by the measured gain (Fig. 3.3). It is important to vary the input charge so that the gain of the system can be observed. The LTSFE chip was designed to have a gain that rolls off with increasing pulse heights. This is observed in the Small Signal Gain graph in Fig 3.3.

3.3 Pulse Shaping

The primary purpose of the pulse shaper is to improve the signal-to-noise ratio by taking advantage of the difference in frequency distribution of the noise and signal. By applying a filter in just the frequency range of the signal, the noise in other frequency bands can be attenuated. In order to make accurate predictions of noise, it is necessary to characterize the shaper output.

An oscilloscope is connected to a pico probe to measure the shaper output directly from the LTSFE chip on the front-end LTSFE board. Using the oscilloscope averaging software, I obtained the output signal in Fig. 3.4. This function will be called our weighting function, W(t), and will determine the shape factors and time constants needed to estimate the noise from the sensor. These shape factors, as seen in Eq. 2.5 are defined in [1] and are shown below.

$$F_i = \frac{1}{2\tau} \int_{-\infty}^{\infty} [W(t)]^2 \, dt. \tag{3.1}$$

$$F_v = \frac{\tau}{2} \int_{-\infty}^{\infty} \left[\frac{dW(t)}{dt} \right]^2 \, dt. \tag{3.2}$$

The time constant, τ, in Eq. 3.1 and Eq. 3.2 refers to the amount of time it takes the signal, ($W(t)$), to go from 10% to 90% of its maximum value. These relations are developed in Semiconductor Detector Systems [1]. As seen, the shape factors F_i and F_v depend on the integral of the weighting function and its derivative. To make these calculations I used ROOT[4] scripts to

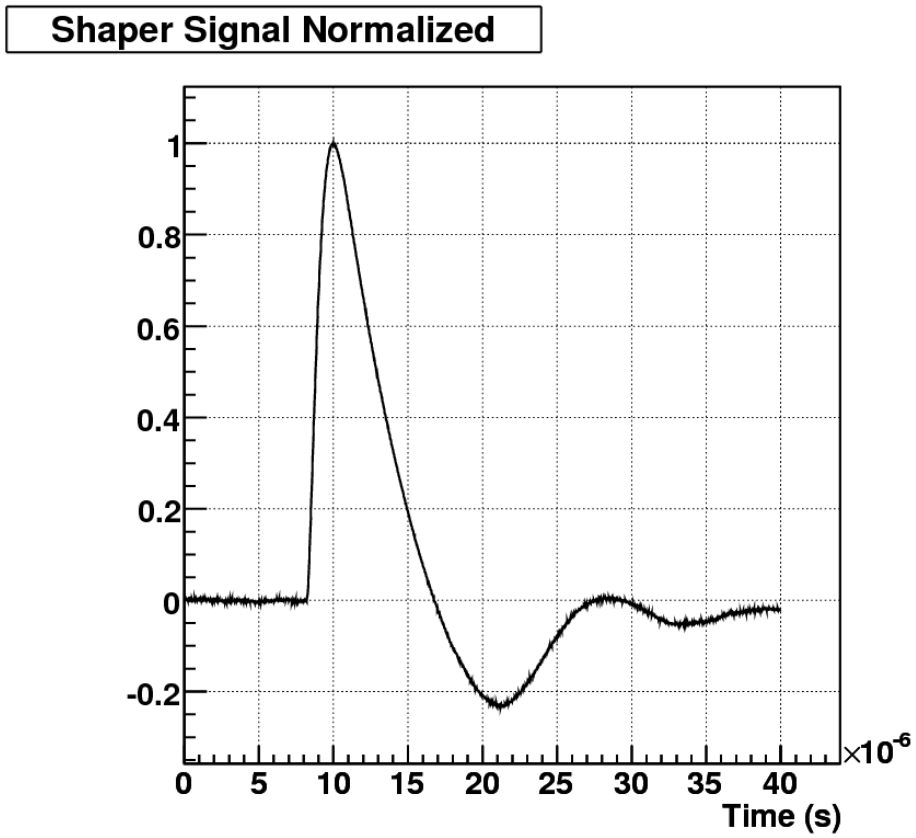

Figure 3.4: Averaged Shaper Signal Output as read from Oscilloscope. Shaper current was 250nA and input voltage was 1.76V. For calculation this is our weighting function W(t)

fit the weighting function, and evaluate its integral numerically[1]. Results are displayed in Table 3.1

Shaper	0.66V	1.32V (pulse heights)
F_i	1.47	1.59
F_v	0.489	0.443
τ (us)	1.06	1.02

Table 3.1: Shape factors and time constants for different pulse heights. Shaping current set to 300nA

The weighting function did not varied significantly with shaper current and pulse height used for my noise measurents; however, The shape factors estimated were very different from those previously used bases on a simple CR-RC shaper ($F_i = F_v = 1$ for CR-RC shaper). These differences proved to be important in our noise estimations. Shaper current had previously been optimized to

[1]These ROOT scipts were written and provided by Vitaliy Fadeyev, PhD, SCIPP

300nA. This was confirmed by examining noise predictions for varied shaper currents. Because it is necessary to vary the input voltage to generate S-curves, the shaping factors for these varying input voltages must be known. By varying the input voltages and holding the shaper current constant at 300nA, weighting functions were measured, and shaping factors were calculated.

3.4 The Sensor

Selectin a sensor and determining method of examining long ladders were two critical decisions in this experiment. The sensor selected was an improperly fabricated DC-biased sensor originally intended for Charge Division[2] studies. DC-biased sensors differ slightly from AC-biased sensors in that the signal transfer between the implant and readout strips is different. For AC-biased sensors, the implant strip is capacitively coupled to the readout strip, while for DC-biased sensors, the implant strip is ohmically coupled to the readout strip. The problem in the fabrication of these Charge Division sensors was the inclusion of a metal readout strip connected and shorting the implant strip every 100um along its length. Readout was supposed to be achieved by connecting just to the ends of the implant. The mistakenly placed readout strip was very thin and therefore had the large value of resistance that is necessary to examine the strip resistance's contribution to noise. While these Charge Division detectors seemed ideal due to the misfabrication, the absence of a large bias resistor and readout coupling capacitor made the service board slightly more complex (discussed in section 3.5).

A previous attempt to measure the noise effects due to strip resistance in long ladder detector systems used GLAST[3] sensors connected in series. This attempt required many sensors and lots of materials to shield and connect them. Unfortunately this attempt did not yield the desired results due to the low resistance of the GLAST readout strips (10Ω/strip). Rather than use many chained together sensors, the idea behind this experiment was to use many of the strips

[2]Charge Division is another detector design intended for the ILC that takes advantage of the long cycling time by reading out sensors from both ends. By measuring the distribution of charge on both ends a longitudinal measurement can be made

[3]GLAST sensors were small scale test structures of the sensors used in the GLAST/FERMI x-ray satellite

on one sensor. The Charge Division sensor had 128 readout strips available at a pitch of 50um. This sensor was ideal not just due to the high resistance of its readout strips, but also due to its geometric similarity to the sensors intended for the long ladder SID design. By connecting the strips in a serpentine arrangement, a much longer sensor can be simulated. With such a large number of readout strips, the only constraint is the ability of the service board to interface to the small 50um pitch.

3.5 The Service Board

In order to have a functioning sensor, both connections to high voltage and ground are needed, as well as a connection between strip readout pads and readout electronics. Due to the unique requirements of the experiment, a custom service board needed to be created. The design and manufacturing of this board proved to be one of the most difficult parts of the experiment. Satial, electronic, and wirebonding constraints yielded the design shown in Fig. 3.5.

Pre-made connectors were available that had been designed for mating to the front-end board. This connector provided high voltage, ground, and eight readout channels. For my purposes only one readout channel was needed. To provide high voltage to the sensor's backside, wirebonds were attached from the connector to the copper side of a piece of copper-plated G10. This piece of G10 previously had much of its copper milled off leaving just the high voltage backside plane and the ground plane as shown in Fig. 3.5. The ground plane was established by connecting wirebonds from the copper plane to the connector. The ground plane's design was developed to provide ground to neighboring strips as well as the adapted bias resistor.

As mentioned in section 3.4, the charge division sensor needed two alterations, the first being an added bias resistor. In common AC-biased sensors each strip is connected to a bias resistor that is connected to ground. This provides a voltage reference for each implant strip, and helps establish the electric field desired in the sensor. Because all the strips on the charge division sensor are floating, a bias resistor needed to be added. The desired location of this resistor is the far

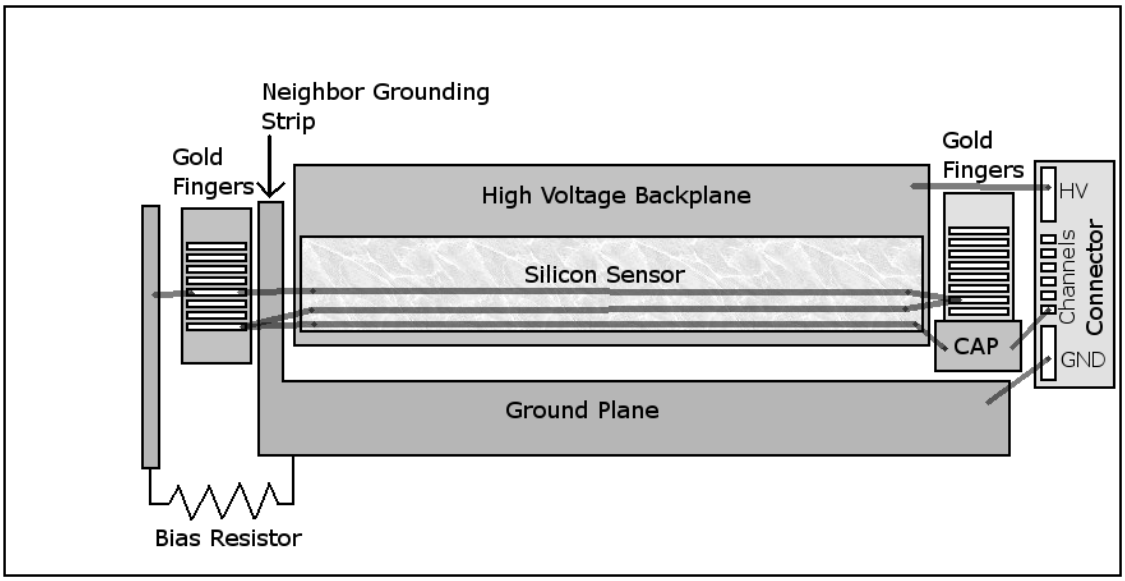

Figure 3.5: The service board used to provide the sensor with high voltage, ground, and readout electronics via the connector.

end(opposite of readout) of the strip, or chain of strips. Most sensors are engineered this way due to spatial constraints on the length of connection (wirebond) between a strip and an amplifier. To best emulate a long ladder sensor, the bias resistor should remain at the far end.

To examining a variety of strip chain lengths, it is easiest to begin with a single strip. Measurements can be made on this strip, then strips can be added lengthening the chain. This requires that it must be relatively easy to move the bias resistor from strip to strip as the end of the chain moves. This necessity brings to light the problem of bonding multiple times to a single sensor pad. Because it is necessary to use a strip's pad for connecting it to adjacent strips in the chain, as well as to the bias resistor, multiple bonds are required for each pad. Bonding more than once to a single pad proved highly unreliable and lead to the possibility of shorts to neighboring strips. To avoid this problem, strips are bonded to thin gold fingers glued next to the sensor. These gold fingers have plenty of area for many bonds allowing the bias resistor to be easily moved, and new strips to be connected to the chain.

The second neccessary alteration to the charge division sensor is a blocking capacitor be-

tween the sensor and readout system. Because only one strip of the chain will be connected to readout, only one capacitor is needed (as seen in Fig. 3.5 labeled 'CAP', 1.5uF). Pieces of gold were soldered to this capacitor so that it could be bonded to the sensor and connector. It is important to note that because the readout connector is on one side of the service board, and the bias resistor is on the other, only strip chains of an odd number of strips can be properly measured. Figure 3.5 shows an example chain of three strips.

The small 50um pitch (spacing between readout strips) of the charge division sensor is very important, and led to many constraints on the service board. Because the long ladders considered in the SID detector design will be approximately 80-100cm (17-21 strips) long, I would ideally like to examine a chain of strips nearly that long. The constraining factor to strip chain length is the pitch of the gold fingers used. The pitch was approximately 500um, or about ten times that of the sensor. Because the sensor had 128 strips, this allowed for 13 strips to be connected in series. While this is less than the length desired, the resistance of the ladders is comparable due to the high resistance of the narrow charge division strips.

The last modification to the sensor is the grounding of neighboring strips. Neighboring strips are those adjacent to the strips being measured in the chain. By grounding these strips, the cross-talk noise component that may compromise results is eliminated. I measured the difference between having neighboring strips grounded, and leaving them floating, to be very slight for single strips. Despite the small difference, every strip added to the chain had its neighboring strips grounded. To ground these strips a thing piece of gold was placed on the edge of the sensor on the bias resistor side. This piece of gold was then connected to the ground plane and wirebonds were connected from neighboring strips to the gold.

4 Results and Analysis

Before making estimations and measurements on the charge division sensor, it is necessary to determine some characteristics of the amplifier. As noted in Eq. 2.5 in section 2.2, i_{na}, e_{na}, and A_f are constants that characterize our amplifier. It is assumed that i_{na} is approximately zero because RC^2 terms dominate for our sensor estimations due to the large resistance and capacitance values. The current fluctuations in the amplifier are small compared with the noise charge generated by voltage fluctuations, e_{na}, and large capacitances ($Q = CV$). Therefore, only two unknowns are left to be determined. Because τ and F_v do not vary significantly, e_{na} and A_f can be taken to be a single constant, β, and solved for using known component values and measurements. Rearranging Eq. 2.5 and dropping i_{na} results in Eq. 4.1. It is simplest, however, to use noise measurements on single capacitors. For a single capacitor Eq. 4.1 becomes 4.2 because $R_s = 0,\ R_b \to \infty$, and $I_d = 0$.

$$\left[\frac{Q^2 - F_i\tau(2eI_d + \frac{4kT}{R_b}) + \frac{F_vC^2}{\tau}4kTR_s}{C^2}\right] = F_v(\frac{1}{\tau}e_{na}^2 + 4A_f) = \beta \tag{4.1}$$

$$\left[\frac{Q^2}{C^2}\right] = F_v(\frac{1}{\tau}e_{na}^2 + 4A_f) = \beta \tag{4.2}$$

The relationship between Q and C can be determined by examining a plot of noise measurements taken at different capacitances. Examining this plot is important because if Q and C are not linearly related, then β will not be well defined. As seen from Fig. 4.1, noise and capacitance are linear for capacitances between 25pF and 200pF. Between 0pF and 25pF there is some nonlinearity; however, examining the capacitance for the charge division sensor (5.2pF/strip), reveals that only

strip lengths under five will be subject to this nonlinearity. Because my primary concern is long strip lengths I will take the slope of this graph between 25 and 200pF to be β. Fitting the data points yields $Q[e] = 393 + 9.1C[pF]$, and therefore $\beta = 9.1\ \frac{e}{pF}$. Rearranging Eq. 4.1 I find Eq. 4.3 below.

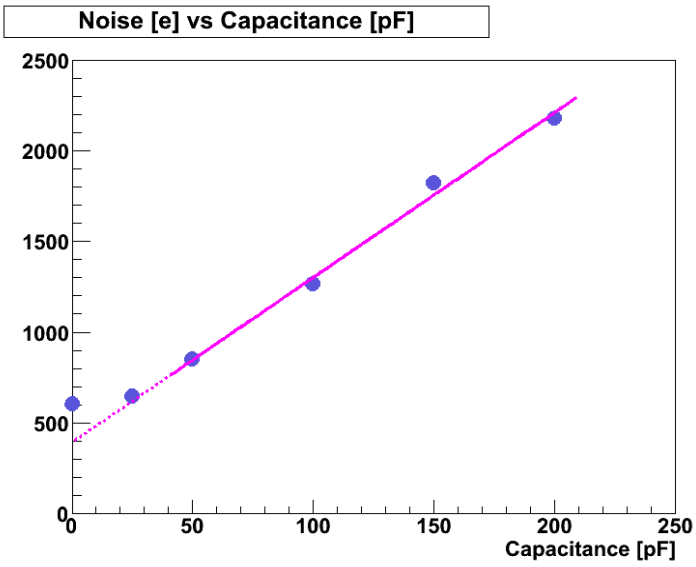

Figure 4.1: Noise measured for different values of capacitance using the LTSFE chip and setup described in section 3.1. Shaper Current set to 300nA

$$Q^2 = F_i\tau(2eI_d + \frac{4kT}{R_b}) + \frac{F_vC^2}{\tau}4kTR_s + F_vC^2\beta \tag{4.3}$$

With the setup intact and understood, the first measurements needed are noise measurements of individual strips on the charge division sensor. Because I cannot measure each strip individually before adding it to the chain, an estimate of the noise variation of strips is needed. Out of the 128 strips on the sensor, only 13 strips are used in the chain (spaced every 10 strips with their neighbors grounded). This leaves a few strips for which it is possible to make individual noise measurements. Spatial constraints limited this measure to only four different strips; however, examining these strips showed that noise measurements did not vary significantly between strips (see Table 4.1).

Strip #	noise(e)
Strip 6	469
Strip 10	456
Strip 15	491
Strip 17	494
Average	477
RMS	18

Table 4.1: Noise measurements for different strips on the charge division sensor. Strip number refers to the number of the strip measured seen on the actual sensor itself.

Now that I know the variance between different strips is low, I can check to see how well these measurements agree with predicted results. Using Eq. 4.3 estimations can be made. For one strip on the charge division sensor with characteristics listed in Table 4.2, the estimated noise value is 446e, which compared with the average noise measurement of strips 6, 10, 15, and 17, is only a 1.7σ difference. This difference may be attributed to the amplifier noise term, i_{na}, which was neglected.

Charge Division Sensor	
I_d (nA)	2.7×10^{-10}
R_b (Ω)	4.40×10^{7}
R_s (Ω)	287
C (F)	5.2×10^{-12}

Table 4.2: Characteristics of the charge division sensor.

Since estimations and measurements appear to agree, more interesting noise measurements on long ladders can be taken. Adding two more strips to the chain (only odd strip numbers can be measured, see section 3.5) yielded a noise measurement of 569e. To make estimations for this three-strip design, it is important to note which sensor characteristics depend on the number of strips. The sensor's strip resistance should add linearly yielding three times the resistance of a single strip. The sensor's capacitance should also add linearly because adding strips to the chain is effectively increasing the surface area that may generate a capacitance. The current leak through the sensor will again add linearly because adding additional strips is just like connecting sensors in series. The bias resistor placed at the end of the sensor will not change value. Using this logic, the estimated

noise of a three strip chain is 580e.

By plotting measurements and estimations of each strip chain length I can see graphically how they agree and differ. The more relevant estimations are those from our rigorous equation that includes amplifier characteristics and shaping factors (Eq. 4.3); however, estimations from the simplified, assumed CR-RC shaper equation (Eq. 2.6)could also be examined to show the inaccuracies of these assumptions at long sensor lengths. Fig. 4.2 shows these estimations alongside actual measurements taken on the charge division sensor for strip chains as long as 13 strips.

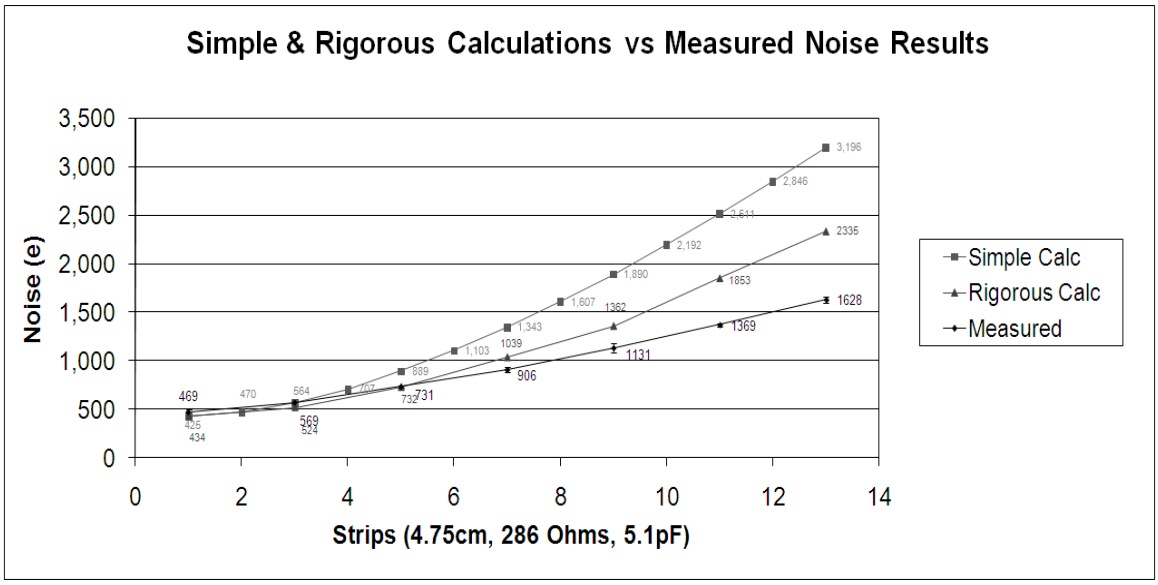

Figure 4.2: A graph of noise estimations and measurements examining each length of the strip chain on the charge division sensor.

My primary concern in this study is the large predicted effect of strip noise at long ladder lengths. The plots displayed below examine how large this effect is relative to other noise sources. Plots 4.3 and 4.4 show the noise generated by strip resistance, bias resistance, current leak, and capacitance. Because noise adds in quadrature, these plots are shown in squared equivalent noise charge. It can be seen that for a single strip length, bias resistance is the dominating factor. When strip lengths increase, capacitance and strip resistance become the two largest terms. As strip lengths continue to grow, strip resistance begins to dominate because noise from strip resistance is

dependent on $l^{2/3}$, while noise from capacitance is dependent only on l (l is the length of the readout strip).

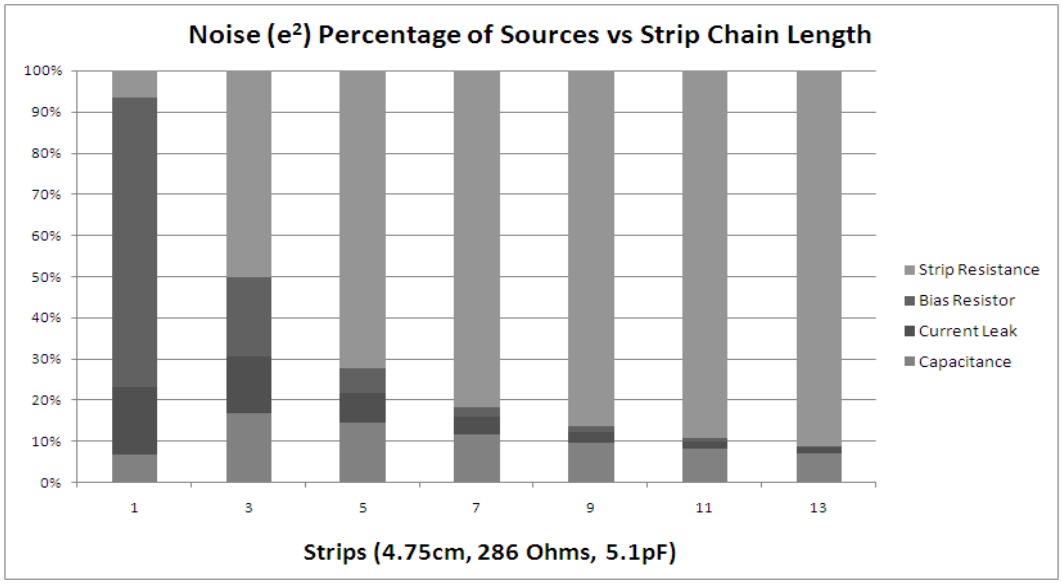

Figure 4.3: A graph of noise estimations from different sources for different strip lengths. Scale is based on percent. Noise values are squared because they add in quadrature.

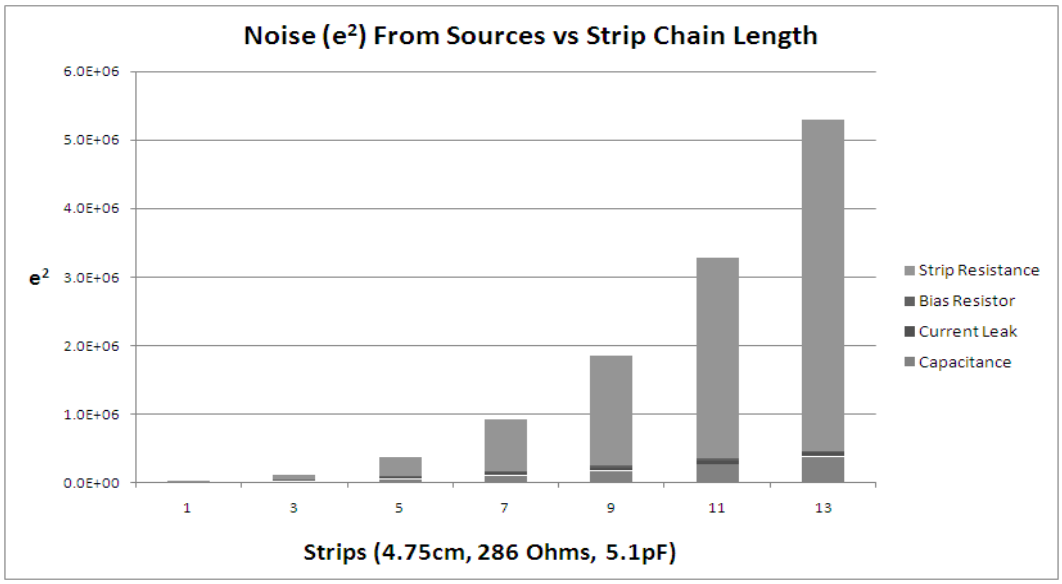

Figure 4.4: A graph of noise estimations from different sources for different strip lengths. Scale is absolute. Noise values are squared because they add in quadrature.

5 Conclusion

Figure 4.2 clearly shows a deviation from the expected measurements. Noise measurements for strip chains longer than five strips are significantly lower than estimations. There is also a sharp difference between rigorous and simplified estimations. This difference emphasizes the importance of amplifier characteristics, and their strong dependence on input pulse heights.

This experimental deviation may mean that there are effects on the noise that are not yet understood. One such effect may be a network effect, which arise in large distributive RC networks. Figure 5.1 shows a simple RC network. If the strip resistance is very large, the capacitor may filter out some of the noise. Each strip on charge division sensor has some capacitance and strip resistance distributed uniformly along the length of the sensor. The Spieler formulae assume a lump resistance and capacitance ignoring these network effects. This assumption is genearlly valid for short sensor lengths, but for the case studied here, it may be incorrect.

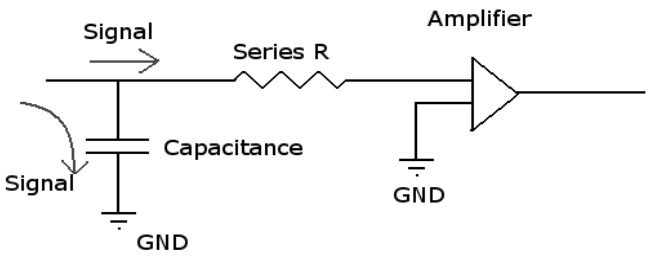

Figure 5.1: Example of RC network.

5.1 Further Studies

A simulation would be helpful to confirm these results. Creating a SPICE (Simulation Program with Integrated Circuit Emphasis) model to estimate the noise for long ladder detector systems would be ideal. Such model was successful for studies of ATLAS ACT sensor performance, where the strip length was short (only 12cm), but the shaping time was ∼50 times smaller (∼25 ns),exacerbating the effect of the strip resistance noise.[5]

A question arising in the experimental design is the location of the input pulse relative to the strip chain. Detectors used in particle accelerators are bombarded with particles at random locations. For this experiment the input pulse was delivered via the connector and therefore always at the readout end of the sensor. If the equivalent noise charge measured is sensitive to the input pulse location, then this experiment is incomplete. If perhaps the signal is attenuated significantly due to the high resistance strips, then another design that would allow the injection of charge at different locations on the chain would be necessary. Charge division studies, conducted in SCIPP labs by Jerome Carman[1], for very high resistance strips (600kΩ), have yielded results that show a noise dependence on charge injection location. While a location dependence study may be experimentally challenging, if future SPICE simulations show a significant location dependence on charge injection, this will be an important future study.

[1] Jerome Carman, UCSC undergraduate, SCIPP. Private communication

Bibliography

[1] Spieler, Helmuth. *Semiconductor Detector Systems*, Oxford University Press, New York, 2005.

[2] *International Linear Collider Design Reference Report.* Vol 4: Detectors, p20. August 2007

[3] J. Phys. G: Nucl. Part. Phys. 33 (2006) 1

[4] ROOT: An object oriented data analysis framework, Rene Brun and Fons Rademakers Linux Journal 998July Issue 51, Metro Link Inc, (English).

[5] Kipnis I., *Noise Analysis due to Strip Resistance in the ATLAS SCT Silicon Strip Module,* LBNL Note 39307, 1996.